Powder Technology 383 (2021) 159–166

Contents lists available at ScienceDirect

Powder Technology

journal homepage: www.elsevier.com/locate/powtec

Image-based prediction of granular flow behaviors in a wedge-shaped hopper by combing DEM and deep learning methods

Zhehan Liao [a], Yizhang Yang [a], Chengfeng Sun [a], Ruiqi Wu [a,b], Ziheng Duan [c], Yueyang Wang [d], Xipeng Li [e], Jian Xu [a,f,*]

[a] College of Materials Science and Engineering, Chongqing University, Chongqing 400044, China
[b] Department of Material Engineering, The University of British Columbia, Vancouver, BC V6T 1Z4, Canada
[c] College of Control Science and Engineering, Zhejiang University, Hangzhou 310027, China
[d] School of Big Data and Software Engineering, Chongqing University, Chongqing 401331, China
[e] NVIDIA China, Beijing 100020, China
[f] Chongqing Key Laboratory of Vanadium-Titanium Metallurgy and Advanced Materials, Chongqing University, Chongqing 400044, China

ARTICLE INFO

Article history:
Received 27 September 2020
Received in revised form 16 January 2021
Accepted 18 January 2021
Available online 21 January 2021

Keywords:
Image-based prediction
DEM
Deep learning
Combined methods
Granular flow
Wedge-shaped hopper

ABSTRACT

Granular flow has solid-, liquid-, or even gas-like behaviors, which can be described through discrete element method (DEM)-based simulations. Although the DEM simulation has advantages in studying particle-scale information, it is computationally intensive. Alternatively, this work proposes to combine the DEM and deep learning methods to predict granular flow behaviors in a wedge-shaped hopper. As the image-based labels are extracted from the DEM simulation, an Alexnet-fully connection (FC) model can make point-to-point predictions about the discharge time. Furthermore, when the first 20% of image-based datasets in the timing sequence are used to train a convolutional neural network (CNN)-long short-term memory (LSTM) network, it can make process predictions about the number ratio of remaining particles (NRRP) in the hopper vs. the discharge time. Although these attempts have some shortcomings at the present stage, more efforts are encouraged to stimulate the future potential of image-based prediction through the combined methods.

1. Introduction

Due to the solid-, liquid-, or even gas-like properties of the granular materials [1,2], the granular flow presents unexpected behaviors, such as segregation [3–7], blockage [8–10] and eccentric flow [11–13] and so on. In order to overcome the difficulties in experimental characterization on aforementioned granular behaviors, Janssen *et al.* [14], as early as 1895, developed a continuum medium model to analyze the particles' static stress of the silo effect, while Adler *et al.* [15] established a molecular dynamics model to track particles' motions. Furthermore, Ogawa [16] introduced the square deviation of velocity fluctuations to characterize the average granular temperature, which was later used to modify the standard dynamic theory of inelastic collisions. Until the 1970s, Cundall and Strack [17] developed the Discrete Element Method (DEM) to analyze rock mechanic problems. Since then, this numerical solution has become one of the most powerful and effective methods of handling various engineering granular problems [18–22] by continuously updating itself for more complex systems [23–28]. Nevertheless, the DEM simulation is computationally intensive, which limits the scale of a simulation [29,30]. Alternatively, machine learning methods have been introduced in recent years to improve the DEM computing efficiency. First of all, the machine learning methods were used to identify and calibrate a set of DEM input parameters by fitting the nonlinear relationship between the dynamic macroscopic particle properties and the DEM parameters [31–34]. Specifically, Benvenuti *et al.* [31] and Ye *et al.* [32] identified the DEM parameters of any given non-cohesive granular materials by training the artificial neural network (ANN) and backpropagation (BP) neural network, respectively. Cheng *et al.* [33] proposed a Bayesian calibration procedure for the DEM modeling of dense granular materials, while Ma *et al.* [34] calibrated the microparameters of the rockfill based on a memetic algorithm with support vector machine (SVM). Second, the machine learning methods were combined to predict different granular flow behaviors [35]. For instance, in order to predict the granular velocity distribution and its influencing factors, Kumar *et al.* [36] selected seven parameters from the DEM simulation, such as the bulk density, the mean diameter, the particle-particle coefficient of friction and so on, as the inputs to train an ANN model. He *et al.* [37] used the relative neighbor particle positions as the inputs to train another ANN network, which improved the accuracy in drag force prediction. Third, the machine learning methods played a

* Corresponding author at: College of Materials Science and Engineering, Chongqing University, Chongqing 400044, China.
E-mail address: jxu@cqu.edu.cn (J. Xu).

https://doi.org/10.1016/j.powtec.2021.01.041
0032-5910/

bridge-like role in the gap between different simulation scales [38], and the machine learning methods were proved to significantly reduce the computational burden while retain the prediction accuracy [39–41].

Although the granular flow has been studied through the combined DEM and machine learning methods, most predications of granular behaviors are data-driven rather than image-driven. However, the continuous real-time images, in comparison to the fetched data, are easier to provide intuitive results without further information extraction. Meanwhile, the deep learning algorithms are found to be very good at image recognition [42]. Therefore, this work focuses on using deep learning methods to predict the granular flow in a wedge-shaped hopper based on the image-based datasets extracted from the DEM simulation. The different initial granular packed patterns are first defined while the corresponding discharge processes are simulated by the DEM. After the relationships between instantaneous granular flow images and the discharge time and the number ratio of remaining particles (NRRP) in the hopper are established, the Alexnet-fully connection (FC) model is proposed to make point-to-point predictions about the discharge time, while the convolutional neural network (CNN)-long short-term memory (LSTM) network is proposed to make process predictions about the NRRP vs. the discharge time.

2. DEM simulation and image-based information collection

2.1. DEM Simulation

Briefly, the principles of DEM are using the Newton equations of motion to describe the translational and rotational motions of each particle, and its details can be found anywhere [21,22,43]. The geometrical dimensions of the wedge-shaped hopper are demonstrated in Fig. 1(a), while the DEM parameters are validated against the experimental measurements reported in our previous works [20,44].

One uniformly mixed bed (denoted by A) and four layer-by-layer mixed beds (denoted by B1 to B4) are defined as the initial binary-sized granular packed patterns in Fig. 1(b). Besides, B1 and B2 have two layers while B3 and B4 have three layers. Eleven randomly changing parameters of five cases in each pattern (twenty-five cases in total), including coefficient of friction i.e. particle-particle ($\mu_{p\text{-}p}$) and particle-wall ($\mu_{p\text{-}w}$), coefficient of restitution i.e. particle-particle ($e_{p\text{-}p}$) and particle-wall ($e_{p\text{-}w}$), and coefficient of rolling friction (μ_r), particle density (ρ), diameter (d), Young's modulus (E), Poisson ratio (υ), number of particles (N), and volume fraction of fine particles (Φ_s), are listed in Table 1. Meanwhile, the shape of particles is spherical and the initial bulk volume in each case keeps constant by taking that of 500 g weighted 6 mm and 2100 kg/m^3 particles as a criterion. Consequently, the DEM simulations are carried out to generate instantaneous granular flow images for the following predictions.

2.2. Labels collection and image-based datasets preparation

As explained in Fig. 2, each instantaneous granular flow image is first extracted from the DEM simulation, and labeled a discharge time which is defined as the time required for the remaining particles in the hopper to discharge completely in the DEM simulation. At the same time, the NRRP is selected as the second label to characterize the granular flow images, and it is determined by Eq. (1).

$$NRRP = \frac{N_r}{N_i} \tag{1}$$

where, N_r represents the number of particles remaining in the hopper obtained from the DEM simulation while N_i represents the initial number of particles in the hopper.

Second, each image is converted into a three-dimensional data matrix, and the transformed datasets are applied to train the selected deep learning models. At last, the trained CNN-FC model realizes the point-to-point prediction of the discharge time, while the trained CNN-LSTM network model achieves the process prediction of the NRRP. In addition, all the DEM simulations are carried out on a workstation equipped with dual Inter Xeon E5-2640v4 (2.4 GHz) CPU, 128 GB RAM, 240 GB SSD, 4 TB hard disk, and Ubuntu 18.04 operating system with LIGGGHTS 3.7.0 [45], while the deep learning training and predicting tasks are accomplished on a workstation equipped with a GTX 1080Ti GPU, Intel Core i7 8700k (3.7 GHz) CPU, 64 GB RAM, 250 GB SSD, 3 TB hard disk, and Ubuntu 18.04 operating system with Pytorch 1.4.0 backend in Python 3.6.

3. Image-based point-to-point prediction of the discharge time

3.1. Image pre-processing and parameter sensitivity analysis

52,353 snapshots of the granular flow in the wedge-shaped hopper are randomly extracted from the front view in the aforementioned twenty-five cases of DEM simulations. Given that the original images' size is (420, 230, 3) in Fig. 3(a), the images are first cropped from the center to a rectangular size (224, 224, 3). The deep learning algorithm then greys these re-shaped images and converts them into a one-dimensional matrix in Fig. 3(b), which is immediately used for the subsequent calculation process. However, before the training process, it is necessary to evaluate the impacts of eleven parameters (refer to Table 1) on the discharge time. Thus, this work employs the gray relational analysis (GRA) [46] as the criteria, and the specific steps are explained as follows:

Step 1: For a given dataset, determine the comparative sequence $X = \{x_{ij,}\ i = 1,2,3\ldots n,\ j = 1,2,3\ldots m\}$ and the reference sequence $Y = \{y_j\}$, where x and y respectively represent parameter' value and the totally discharge time which represents the discharge time of the initial packed stage, while the subscripts i and j respectively represent different parameters and cases.

Step 2: Normalize both sequences by the initialization normalization method (Eqs. (2) and (3)).

$$x_{ij}' = \frac{x_{ij}}{x_{i1}} \tag{2}$$

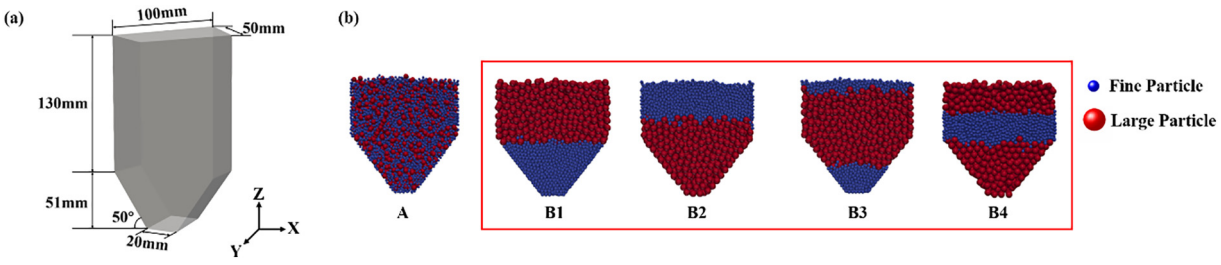

Fig. 1. DEM simulation conditions: (a) the geometrical dimensions of the wedge-shape hopper and (b) the uniformly mixed (A type) and layer-by-layer mixed (B1-B4 type) binary-sized granular packed patterns initialized in the hopper.

Table 1
The randomly changing parameters for the DEM simulation under five initial granular packed patterns.

No.	N (−)	υ (−)	E (GPa)	Φ_s(−)	$e_{p\text{-}p}$ (−)	$e_{w\text{-}p}$ (−)	$\mu_{p\text{-}p}$ (−)	$\mu_{w\text{-}p}$ (−)	μ_r (−)	$d(mm)$	ρ(kg/m^3)
A-1	620	0.35	0.01	0.2	0.3	0.1	0.5	0.2	0.08	6,9	2800
A-2	10,180	0.26	0.375	0.5	0.5	0.8	0.6	0.7	0.02	3,6	2100
A-3	5450	0.42	0.065	0.2	0.4	0.7	0.9	0.2	0.05	3,6	1800
A-4	14,700	0.3	0.01	0.8	0.7	0.3	0.2	0.9	0.07	3,9	2500
A-5	7900	0.4	0.01	0.4	0.9	0.1	0.7	0.1	0.01	3,9	2800
B1-1	6875	0.42	0.01	0.3	0.9	0.9	0.3	0.3	0.06	3,6	1500
B1-2	7596	0.33	0.01	0.4	0.4	0.8	0.4	0.2	0.03	3,9	1500
B1-3	1239	0.42	0.01	0.4	0.3	0.5	0.2	0.1	0.08	6,9	1800
B1-4	2394	0.3	0.375	0.1	0.7	0.1	0.4	0.5	0.08	3,9	2100
B1-5	8464	0.4	0.065	0.4	0.5	0.3	0.5	0.9	0.06	3,6	2800
B2-1	1239	0.26	0.375	0.4	0.6	0.7	0.5	0.7	0.04	6,9	2800
B2-2	3696	0.45	0.01	0.1	0.2	0.2	0.9	0.2	0.09	3,6	2500
B2-3	8464	0.35	0.01	0.4	0.8	0.2	0.5	0.8	0.06	3,6	2100
B2-4	1094	0.3	0.01	0.3	0.9	0.9	0.1	0.7	0.01	6,9	2100
B2-5	9330	0.4	0.2	0.5	0.1	0.1	0.8	0.2	0.02	3,9	1800
B3-1	5285	0.26	0.01	0.2	0.6	0.3	0.3	0.2	0.01	3,6	2500
B3-2	4128	0.4	0.2	0.2	0.7	0.1	0.3	0.1	0.07	3,9	2800
B3-3	950	0.4	0.375	0.2	0.3	0.1	0.2	0.1	0.09	6,9	2100
B3-4	5862	0.35	0.065	0.3	0.9	0.8	0.6	0.6	0.04	3,9	2100
B3-5	5170	0.35	0.2	0.2	0.8	0.9	0.8	0.9	0.02	3,6	2800
B4-1	6874	0.35	0.2	0.3	0.8	0.4	0.9	0.3	0.02	3,6	1500
B4-2	9330	0.33	0.01	0.5	0.6	0.1	0.6	0.8	0.04	3,9	2500
B4-3	805	0.2	0.375	0.1	0.1	0.9	0.1	0.1	0.05	6,9	2100
B4-4	1094	0.2	0.065	0.3	0.5	0.5	0.2	0.8	0.09	6,9	2100
B4-5	4128	0.2	0.375	0.2	0.9	0.2	0.3	0.9	0.08	3,9	2100

$$y_j' = \frac{y_j}{y_1} \tag{3}$$

Step 3: Calculate the grey relational coefficient (Eq. (4)).

$$\xi_{ij} = \frac{\min\limits_i \min\limits_j |y_j' - x_{ij}'| + \rho * \max\limits_i \max\limits_j |y_j' - x_{ij}'|}{|y_j' - x_{ij}'| + \rho * \max\limits_i \max\limits_j |y_j' - x_{ij}'|} \tag{4}$$

where ρ is the distinguishing coefficient, ρ∈[0,1], which is 0.5 in this work.

Step 4: Calculate the GRA grade r (Eq. (5)).

$$r_i(X_i, Y) = \frac{1}{m}\sum_{j=1}^{m} \xi_{ij} \tag{5}$$

Step 5: Calculate the percentage weight of each parameter based on GRA grade (Eq. (6))

$$p_i = \frac{r_i(X_i, Y)}{\sum\limits_{i=1}^{n} r_i(X_i, Y)} \times 100\% \tag{6}$$

The percentage weights to evaluate the impacts of eleven parameters on the discharge time in different cases are depicted and compared in Fig. 3(c), in which the mean results are highlighted in the middle. Although the particle diameter out of the eleven parameters has the greatest influence on the discharge time (11.14%) while the particle Young's modulus has the least impact (7.17%), all the selected parameters under present conditions make comparable contributions to the discharge time.

3.2. Selection of training models

All the image-based datasets after pre-processing are randomly classified into training group (60%), testing group (20%), and cross

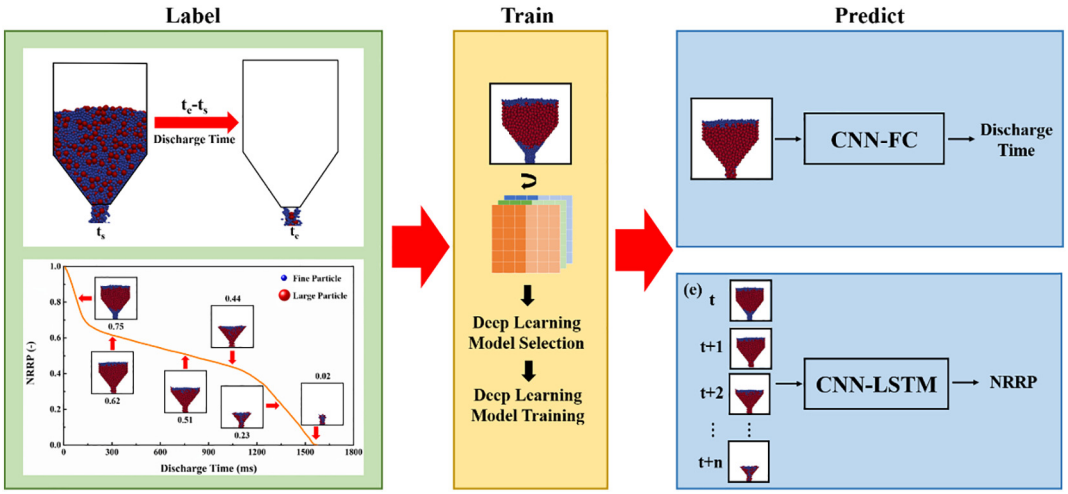

Fig. 2. The flow diagram of proposed the DEM and deep learning combined methods.

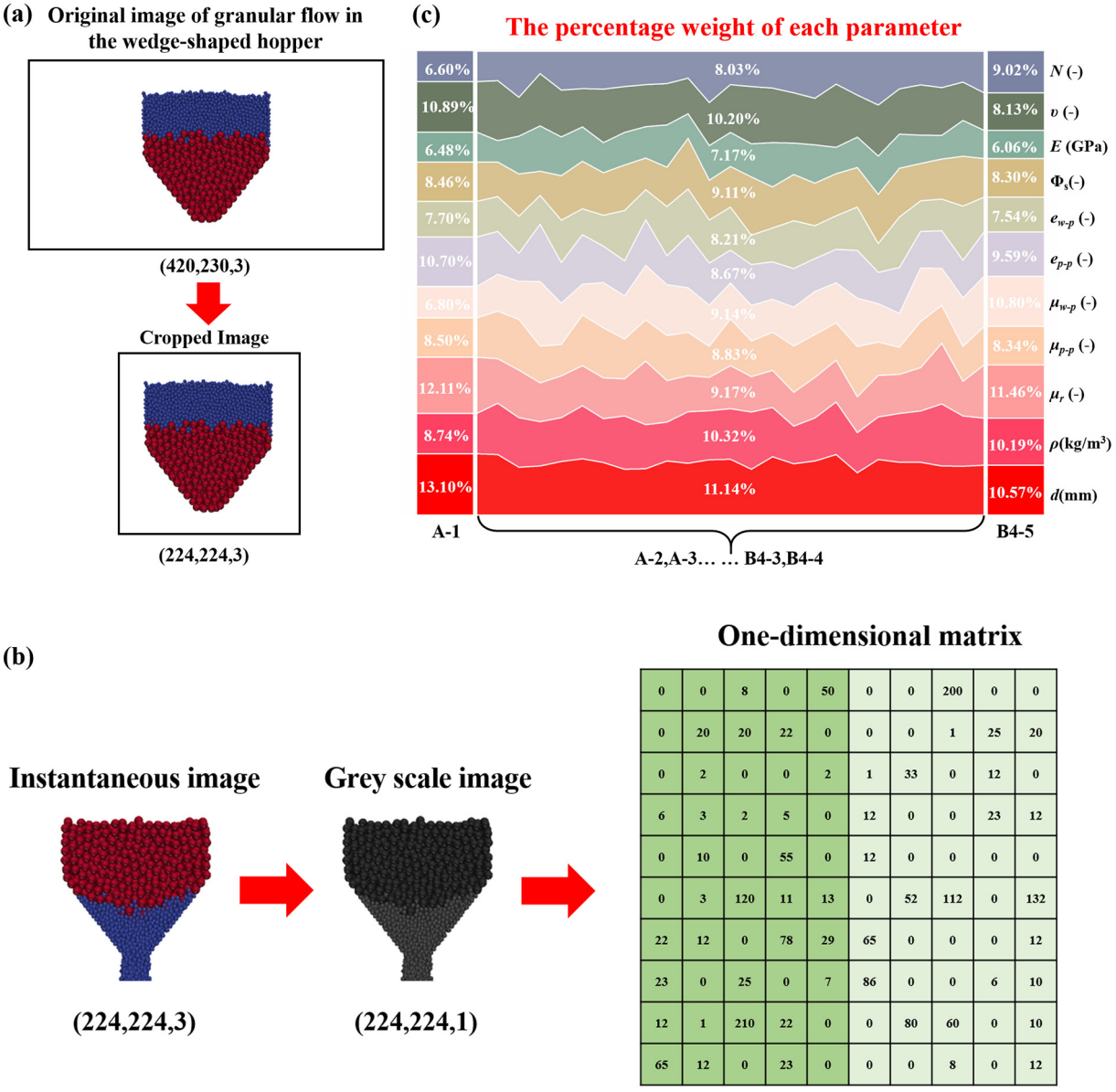

Fig. 3. (a) The image pre-processing by re-shaping its size, (b) the explanations on greying the instantaneous image and converting it into a one-dimensional matrix, and (c) evaluating the influences of eleven parameters on the discharge time by the GRA method.

validation group (20%). Then those dataset in the first group are used to train four CNN models, including Alexnet [47], Resnet-50 [48], VGG-16 and VGG-19 [49]. Thereafter, the trained models are applied to test and validate, and their predicted results are compared to the datasets in the validation group in Fig. 4, and the further quantitative comparisons in terms of mean absolute error (MAE, Eq. (7)), root mean square error (RMSE, Eq. (8)) and determination coefficient (R^2, Eq. (9)), are summarized in Table 2. The Alexnet model, which has the minimum MAE, RMSE values and the maximum R^2 value, is considered as the best CNN candidate for the following prediction.

$$\mathrm{MAE} = \frac{1}{m}\sum_{i=1}^{m}|y_i - \hat{y}_i| \tag{7}$$

$$RMSE = \sqrt{\frac{1}{m}\sum_{i=1}^{m}(y_i - \hat{y}_i)^2} \tag{8}$$

$$R^2 = 1 - \frac{\sum_{i=1}^{m}(y_i - \hat{y}_i)^2}{\sum_{i=1}^{m}(y_i - \bar{y}_i)^2} \tag{9}$$

where, m is the predicted length, and y_i, $\hat{y}_i$, and $\bar{y}_i$ respectively represent the predicted value, the observed values, and the average value.

3.3. Proposed architecture for the point-to-point prediction

The above-selected Alexnet model is combined with the FC model to establish an Alexnet-FC model to predict the discharge time, and its architecture is explained in Fig. 5. In short, the left part employs the Alexnet model to extract the features from the input images, while the right part makes use of the FC model to analyze those features. As a result, the discharge time of granular flow in a wedge-shaped hopper can

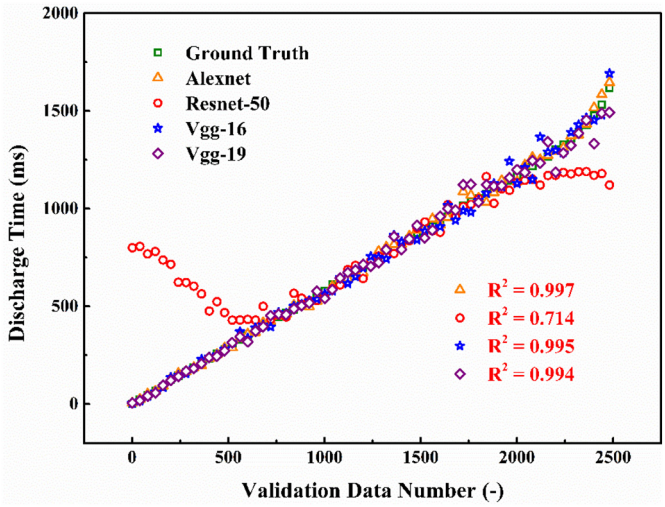

Fig. 4. The comparison between the discharge times predicted by four CNN models and validation datasets.

Table 2
The quantitative comparisons of the four CNN models' prediction performance.

	Alexnet	Resnet-50	Vgg-16	Vgg-19
MAE	46.617	358.937	50.336	62.751
RMSE	61.286	513.528	71.685	90.607
R^2	0.997	0.714	0.995	0.994

be predicted by feeding the proposed model with an arbitrary granular flow image.

As a result, the predicted discharge times under five initial packed patterns in the wedge-shaped hopper (refer to Fig. 1(b)) are compared with the ground truth or observed values in Fig. 6, and the average relative errors are calculated (Eq. (10)) and shown in the insets. All the R^2 values reach 0.997 or above, while the maximum of average relative errors is 0.063. These results substantially prove that the proposed Alexnet-FC model have excellent point-to-point prediction of the discharge time corresponding to any instantaneous image of granular flow in a wedge-shaped hopper.

$$|\overline{Error}| = \frac{1}{m}\sum_{i=1}^{m}\frac{|y_i - \hat{y}_i|}{\hat{y}_i} \tag{10}$$

where, m is the predicted length, y_i denotes the predicted values, and $\hat{y}_i$ represents the ground truth or observed values.

4. Image-based process prediction of the NRRP

4.1. Description of the process prediction

Although the Alexnet-FC model in the previous section achieves the point-to-point prediction of the discharge time, the process prediction of the granular flow in the timing sequence is of greater interest for practical applications. Therefore, the datasets of the NRRP, as defined in the Section 2.2, are also extracted from the DEM simulated images, and then they are sorted in a timing sequence rather than a random or arbitrary sequence used in the previous section. In the first step, only the first 20% of the NRRP datasets are employed to train the model. Then the trained model would automatically predict the NRRP distribution with the discharge time. The average relative errors between the predicted NRRP and simulated values are also calculated to evaluate the prediction performance for the remaining process.

4.2. Proposed architecture for the process prediction

The LSTM network is an improved recurrent neural network (RNN) [50]. Its basic unit is composed of the forget gate, input gate and output gate, and the corresponding equations can be found in any LSTM related deep learning literature [51,52]. This work uses the CNN-LSTM combined network to make the process prediction, and its architecture is explained in Fig. 7. The CNN part is responsible for the image features extraction, while the LSTM part is in charge of the NRRP prediction. To be more specific, the CNN has four convolutional layers (Conv2D), and the numbers of convolution kernels in each layer are 32, 64, 128 and 25, respectively. The flatten operation is then performed to extract the global features, which compress a three-dimensional vector array to a one-dimensional vector array having 1024 elements. At last, four layers of LSTM are connected in the back, and the numbers of neurons in each layer are 4, 8, 16, and 32, respectively.

As a result, the training and predicting NRRP distributions under five initial packed patterns in the wedge-shaped hopper (refer to Fig. 1(b)) with the discharge time are depicted in Fig. 8. There are three points worthy to be noted. First, all the predicted NRRPs with the discharge

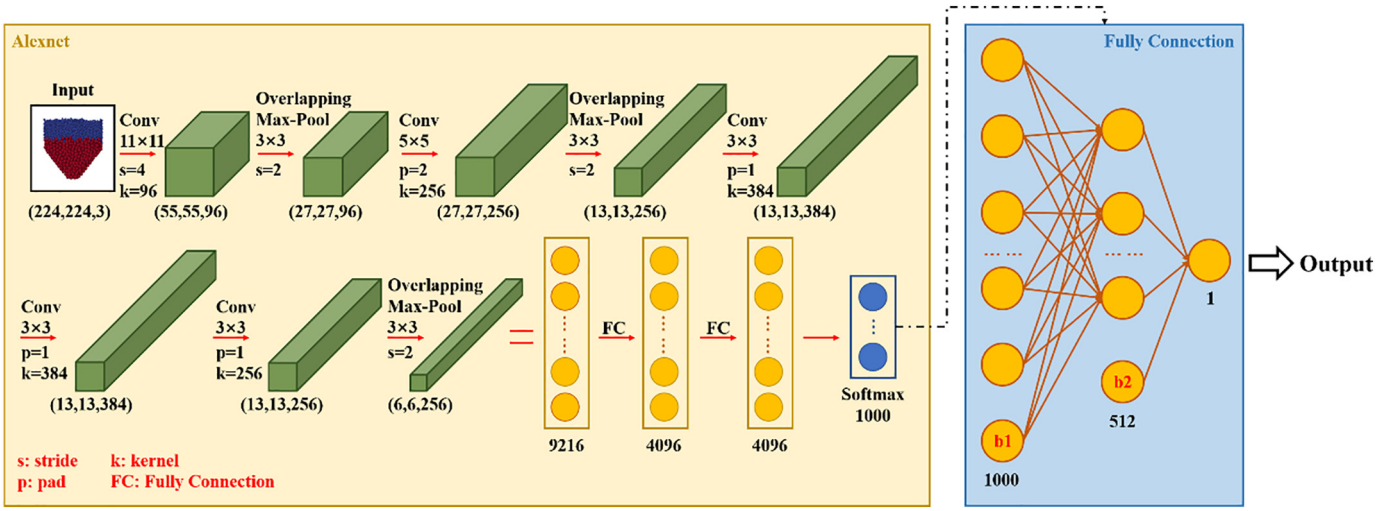

Fig. 5. The proposed architecture combing the Alexnet and FC models for the point-to-point prediction.

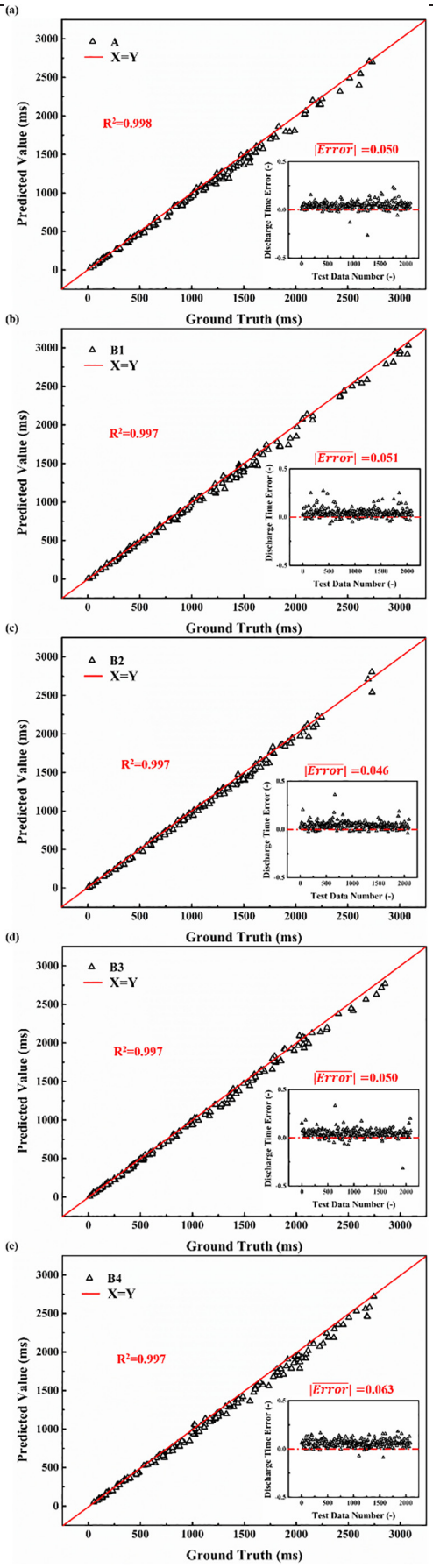

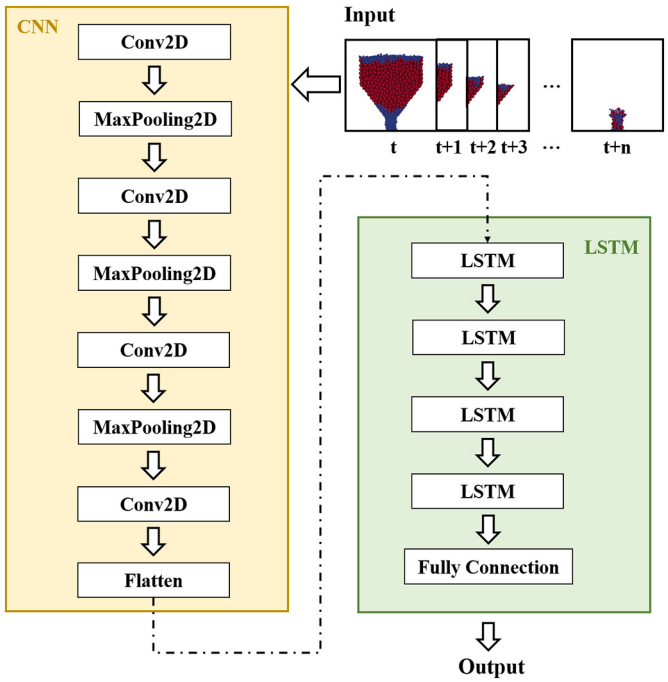

Fig. 7. The proposed architecture combing CNN and LSTM networks for process prediction.

time have the similar trends as simulated by the DEM. Second, the predicted results from the very beginning to the certain stage by the proposed CNN-LSTM model are quite consistent with the DEM simulated results, when the initial granular packed patterns are A, B2 and B3 types. Then the obvious deviations are noticed from the discharge time at 1387 ms, 2163 ms and 1180 ms, respectively. Nevertheless, the minimum average relative error in the three cases is 0.082. Third, when the initial granular packed patters are B1 and B4 types, the deviations between the predicted and simulated NRRPs increase from the beginning of predicted stage. Therefore, their average relative errors exceed 0.39.

Besides, taking the B2-1 case as an example, Fig. 9 shows that the total CPU-hour spent on the DEM simulation is 4500 s. In contrast, the image-based data collection from the DEM simulation costs 900 s, while the subsequent model training and prediction respectively costs 197 s and 12 s. It means the total CPU-hour spent on the CNN-LSTM prediction based on the DEM simulation is 1109s under present conditions. Therefore, the proposed DEM-deep learning combined method can save about 3/4 of the DEM simulation time in this case.

Overall, the proposed CNN-LSTM model to some extent has the capability of the process prediction and presents a great potential for saving computation resource. However, more efforts on the parameters optimization, the image pre-processing, the dataset diversity, and so on, should be devoted to driving the application of the image-based prediction in the future.

5. Conclusions

The deep learning-assisted prediction has advantages over the DEM alone in the computing efficiency, the large-scale simulation solution, and so on. Based on the extracted labels from the instantaneous DEM simulated images, this work introduces the Alexnet-FC model and CNN-LSTM model respectively to make the point-to-point and process

Fig. 6. The comparison between the predicted discharge times of granular flow under five initial packed patterns in the wedge-shaped hopper (a) A; (b) B1; (c) B2; (d) B3; (e) B4 and the corresponding ground truth or observed values.

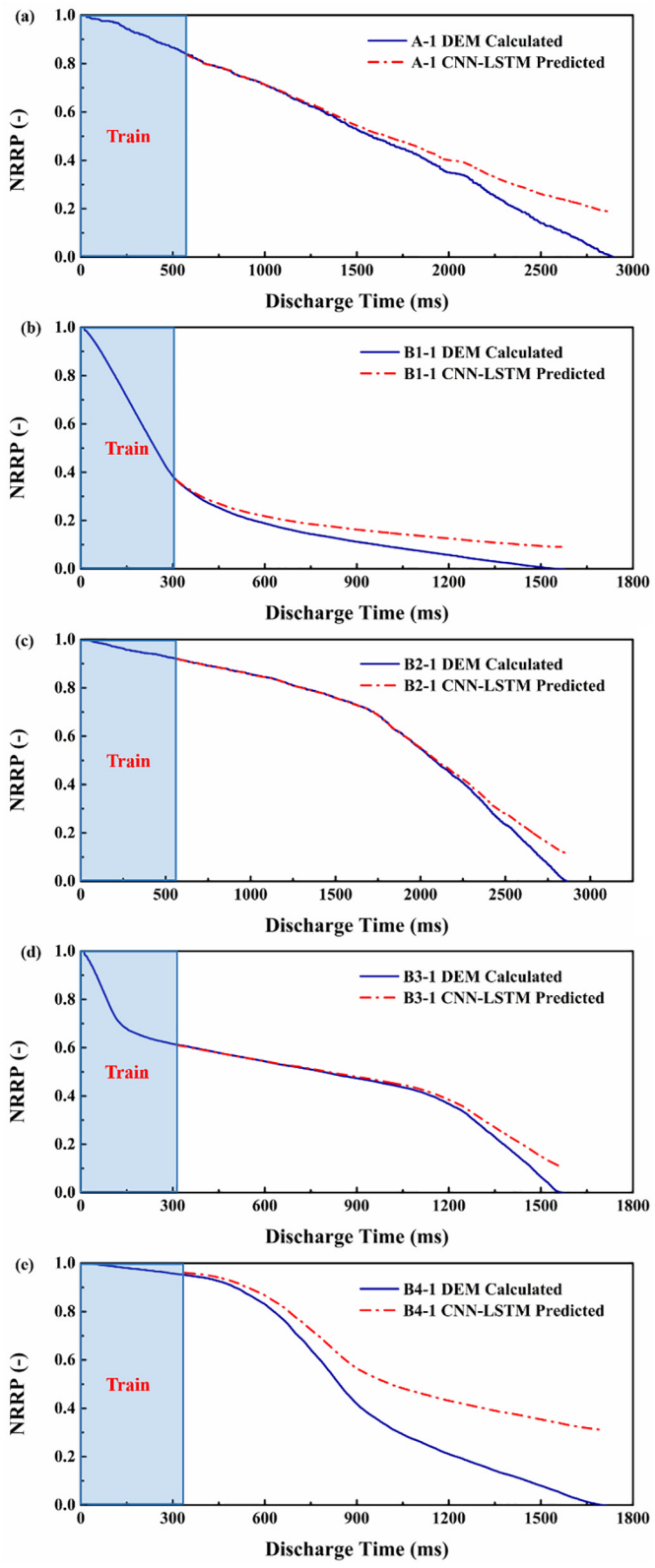

Fig. 8. The comparison between the predicted NRRPs vs. the discharge time and the DEM simulated results under five initial packed patterns in the wedge-shaped hopper (a) A-1; (b) B1-1; (c) B2-1; (d) B3-1; (e) B4-1.

predictions about granular flow behaviors in a wedge-shaped hopper. The main findings under present conditions are highlighted as follows:

(1) Although the spherical particle diameter has the greatest influence on the discharge time whereas the Young's modulus has the least influence, all the selected parameters make comparable contributions to the discharge time. Accordingly, the Alexnet-FC model is proposed and proved to have the excellent ability of the point-to-point prediction about the discharge time corresponding to any instantaneous granular flow images.

(2) The CNN-LSTM model is proposed to use the first 20% of image-based datasets in the timing sequence for training, and then the trained network to some extent has the capability of the process prediction about the NRRP distribution with the discharge time. The proposed method can save about 3/4 of the total CPU-hour spent on the DEM simulation alone under present conditions. This work demonstrates great potential of combing the DEM and deep learning methods to drive the image-based prediction, when more works on the parameters optimization, the image preprocess technique, the dataset diversity, and so on, need to be done in the future.

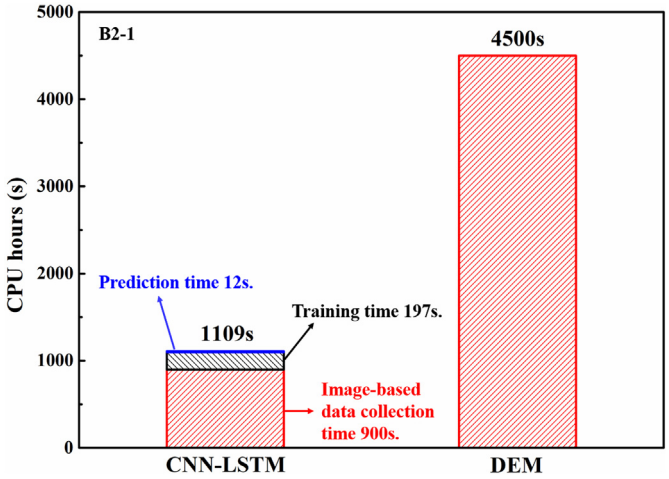

Fig. 9. The comparison on the spent CPU-hour between the combined CNN-LSTM method and the DEM simulation alone.

Declaration of Competing Interest

None.

Acknowledgments

The authors gratefully acknowledge funding through projects from the Fundamental Research Funds for the Central Universities (2020CDJQY-A005), the Natural Science Foundation of Chongqing, China (cstc2019jcyj-msxmX0089) and the Young Top-notch Talent Program of Chongqing, China (CQYC2020057673), Z.L. acknowledges the Graduate Scientific Research and Innovation Foundation of Chongqing, China (CYS19035).

References

[1] X.M. Zheng, J.M. Hill, Molecular dynamics simulation of granular flows: slip along rough inclined planes, Comput. Mech. 22 (1998) 160–166.

[2] R. Freeman, Measuring the flow properties of consolidated, conditioned and aerated powders — A comparative study using a powder rheometer and a rotational shear cell, Powder Technol. 174 (2007) 25–33.

[3] S. Wu, M. Kou, J. Xu, X. Guo, K. Du, S. Wei, S. Jing, DEM simulation of particle size segregation behavior during charging into and discharging from a Paul-Wurth type hopper, Chem. Eng. Sci. 99 (2013) 314–323.

[4] D. Wu, P. Zhou, H. Yan, P. Shi, C.Q. Zhou, Numerical investigation of the effects of size segregation on pulverized coal combustion in a blast furnace, Powder Technol. 342 (2019) 41–53.

[5] C.C. Liao, Effect of dynamic properties on density-driven granular segregation in a rotating drum, Powder Technol. 345 (2019) 151–158.

[6] S.Y. He, J.Q. Gan, D. Pinson, Z.Y. Zhou, Particle shape-induced radial segregation of binary mixtures in a rotating drum, Powder Technol. 341 (2019) 157–166.
[7] M. Alizadeh, A. Hassanpour, M. Pasha, M. Ghadiri, A. Bayly, The effect of particle shape on predicted segregation in binary powder mixtures, Powder Technol. 319 (2017) 313–322.
[8] P. Bunchatheeravate, J. Curtis, Y. Fujii, S. Matsusaka, Prediction of particle charging in a dilute pneumatic conveying system, AIChE J. 59 (2013) 2308–2316.
[9] K.M. Forward, D.J. Lacks, R.M. Sankaran, Triboelectric charging of granular insulator mixtures due solely to particle-particle interactions, Ind. Eng. Chem. Res. 48 (2009) 2309–2314.
[10] T. Umekage, S. Yuu, T. Shinkai, T. Abe, Numerical simulation for blockage of cohesive particles in a hopper using the distinct element method and its correlation with experimental results of real cohesive granular materials, Adv. Powder Technol. 9 (1998) 331–344.
[11] J.A. Pita, S. Sundaresan, Developing flow of a gas-particle mixture in a vertical riser, AIChE J. 39 (1993) 541–552.
[12] I. Sielamowicz, M. Czech, T.A. Kowalewski, Empirical description of flow parameters in eccentric flow inside a silo model, Powder Technol. 198 (2010) 381–394.
[13] I. Sielamowicz, A. Czech, T.A. Kowalewski, Comparative analysis of empirical descriptions of eccentric flow in silo model by the linear and nonlinear regressions, Powder Technol. 270 (2015) 393–410.
[14] H.A. Janssen, Z. Vereins, DeutschIng 39 (1895) 1045.
[15] B.J. Alder, W. T. E, Phase transition for a hard sphere system, J. Chem. Phys. 27 (5) (1957) 1208.
[16] S. Ogawa, Multitemperature theory of granular materials, Proc. US-Japan Seminar on Continuum-Mechanical and Statistical Approaches in the Mechanics of Granular Materials 1978, pp. 208–217.
[17] P.A. Cundall, O. Strack, Discussion: a discrete numerical model for granular assemblies, Geotechnique 30 (1980) 331–336.
[18] A. Mahmood, M. Elektorowicz, A review of discrete element method research on particulate systems, IOP Conf. Series Mater. Sci. Eng. 136 (2016), 012034, .
[19] Y. Guo, J.S. Curtis, Discrete element method simulations for complex granular flows, Annu. Rev. Fluid Mech. 47 (2015) 21–46.
[20] J. Xu, Z. Hu, Y. Xu, D. Wang, L. Wen, C. Bai, Transient local segregation grids of binary size particles discharged from a wedge-shaped hopper, Powder Technol. 308 (2017) 273–289.
[21] Y. Xu, J. Xu, Z. Liao, Y. Pei, L. Gao, C. Sun, M. Kou, L. Wen, DEM study on ternary-sized particle segregation during the sinter burden charging process, Powder Technol. 343 (2019) 422–435.
[22] Y. Xu, J. Xu, C. Sun, K. Ma, S. Cheng, L. Wen, S. Zhang, C. Bai, Quantitative comparison of binary particle mass and size segregation between serial and parallel type hoppers of blast furnace bell-less top charging system, Powder Technol. 328 (2018) 245–255.
[23] A.K. Olaleye, O. Shardt, G.M. Walker, H.E.A. Van den Akker, Pneumatic conveying of cohesive dairy powder: experiments and CFD-DEM simulations, Powder Technol. 357 (2019) 193–213.
[24] A. Zang, W.T. F, Elastic stiffness and stress concentration in cemented granular material, Int. J. Rock Mech. Min. Sci. Geomech. Abstr. 32 (6) (1995) 563–574.
[25] R. Hesse, F. Krull, S. Antonyuk, Experimentally calibrated CFD-DEM study of air impairment during powder discharge for varying hopper configurations, Powder Technol. 372 (2020) 404–419.
[26] M. Sousani, A.M. Hobbs, A. Anderson, R. Wood, Accelerated heat transfer simulations using coupled DEM and CFD, Powder Technol. 357 (2019) 367–376.
[27] R. Lu, L. Zhang, P. Ricoux, L. Wang, Experiments and CFD-DEM simulations of cohesive particles sedimentation in stilled fluid, Powder Technol. 356 (2019) 222–230.
[28] J. Baxter, H. Abou-Chakra, U. TüZün, B. Mills Lamptey, A DEM simulation and experimental strategy for solving fine powder flow problems, Chem. Eng. Res. Des. 78 (2000) 1019–1025.
[29] M. Sakai, S. Koshizuka, Large-scale discrete element modeling in pneumatic conveying, Chem. Eng. Sci. 64 (2009) 533–539.
[30] K. Washino, C.H. Hsu, T. Kawaguchi, Y. Tsuji, Similarity model for DEM simulation of fluidized bed, J. Soc. Powder Technol. Japan 44 (2010) 198–205.
[31] L. Benvenuti, C. Kloss, S. Pirker, Identification of DEM simulation parameters by artificial neural networks and bulk experiments, Powder Technol. 291 (2016) 456–465.
[32] F. Ye, C. Wheeler, B. Chen, J. Hu, K. Chen, W. Chen, Calibration and verification of DEM parameters for dynamic particle flow conditions using a backpropagation neural network, Adv. Powder Technol. 30 (2019) 292–301.
[33] H. Cheng, T. Shuku, K. Thoeni, P. Tempone, S. Luding, V. Magnanimo, An iterative Bayesian filtering framework for fast and automated calibration of DEM models, Comput. Methods Appl. Mech. Eng. 350 (2019) 268–294.
[34] C. Ma, J. Yang, G. Zenz, E.J. Staudacher, L. Cheng, Calibration of the microparameters of the discrete element method using a relevance vector machine and its application to rockfill materials, Adv. Eng. Softw. 147 (2020) 102833.
[35] A.R. Peeketi, R.K. Desu, P. Kumbhar, R.K. Annabattula, Thermal analysis of large granular assemblies using a hierarchical approach coupling the macro-scale finite element method and micro-scale discrete element method through artificial neural networks, Comput. Particle Mech. 6 (2019) 811–822.
[36] R. Kumar, C.M. Patel, A.K. Jana, S.R. Gopireddy, Prediction of hopper discharge rate using combined discrete element method and artificial neural network, Adv. Powder Technol. 29 (2018) 2822–2834.
[37] L. He, D.K. Tafti, A supervised machine learning approach for predicting variable drag forces on spherical particles in suspension, Powder Technol. 345 (2019) 379–389.
[38] H.Q. Do, A.M. Aragón, D.L. Schott, A calibration framework for discrete element model parameters using genetic algorithms, Adv. Powder Technol. 29 (2018) 1393–1403.
[39] D. Barrasso, A. Tamrakar, R. Ramachandran, A reduced order PBM–ANN model of a multi-scale PBM–DEM description of a wet granulation process, Chem. Eng. Sci. 119 (2014) 319–329.
[40] P. Kumar, K. Sinha, N. Nere, Y. Shin, R. Ho, A. Sheikh, L. Mlinar, A machine learning framework for computationally expensive transient models, Sci. Rep. 10 (2020) 11492.
[41] H. Wu, S. Hao, A deep neural network model of particle thermal radiation in packed bed, Proc. AAAI Conf. Artific. Intell. 34 (2020) 1029–1036.
[42] M.R. Minar, J. Naher, Recent Advances in Deep Learning: An Overview, 2018.
[43] C. Sun, J. Xu, Z. Liao, Y. Xu, M. Kou, L. Wen, Causes of particle trajectory fluctuation on the rotating chute in circumferential direction at bell-less top with parallel type hoppers, ISIJ Int. 59 (2019) 1527–1533.
[44] Z. Liao, J. Xu, C. Sun, Y. Xu, Y. Pei, M. Kou, Z. Hu, L. Meng, L. Wen, Influence of particle packed pattern on the transient granular flow in a wedge-shaped hopper, Adv. Powder Technol. 31 (2020) 670–677.
[45] Kloss Christoph, Goniva Christoph, Hager Alice, Amberger Stefan, Pirker Stefan, Models, algorithms and validation for opensource DEM and CFD-DEM, Progr. Comput. Fluid Dynam. Int. J. 12 (2012) 140–152.
[46] Y. Kuo, T. Yang, G.W. Huang, The use of grey relational analysis in solving multiple attribute decision-making problems, Comput. Ind. Eng. 55 (2008) 80–93.
[47] A. Krizhevsky, I. Sutskever, G. Hinton, ImageNet Classification with Deep Convolutional Neural Networks, International Conference on Neural Information Processing Systems, 2012.
[48] K. He, X. Zhang, S. Ren, S. Jian, Deep Residual Learning for Image Recognition, IEEE Conference on Computer Vision & Pattern Recognition, 2016.
[49] K. Simonyan, A. Zisserman, Very deep convolutional networks for large-scale image recognition, Comput. Therm. Sci. (2015) 1409–1556.
[50] R.J. Williams, D. Zipser, A learning algorithm for continually running fully recurrent neural networks, Neural Comput. 1 (2014) 270–280.
[51] F.A. Gers, J. Schmidhuber, F. Cummins, Learning to forget: continual prediction with LSTM, Neural Comput. 12 (2000) 2451–2471.
[52] Y. Tan, G. Zhao, Transfer learning with long short-term memory network for state-of-health prediction of lithium-ion batteries, IEEE Trans. Ind. Electron. 67 (10) (2019) 8723–8731.